RSC Advances

ROYAL SOCIETY OF CHEMISTRY

www.rsc.org/advances

Cite this: DOI: 10.1039/c0xx00000x

www.rsc.org/xxxxxx

ARTICLE TYPE

Tuning optical and dielectric properties of calcium copper titanate $Ca_xCu_{3-x}Ti_4O_{12}$ nanopowders

Ali Omar Turky[*a,c], Mohamed Mohamed Rashad[a], Zaki Ismail Zaki[a,b], Ibrahim Ahmed Ibrahim[a], Mikhael Bechelany[c]

Received (in XXX, XXX) XthXXXXXXXXX 20XX, Accepted Xth XXXXXXXXX 20XX
DOI: 10.1039/b000000x

Calcium copper titanate $Ca_xCu_{3-x}Ti_4O_{12}$ (CCTO) nanopowders have been synthesized using organic acid precursor method based on commercially available materials. The results revealed that cubic CCTO phase was accomplished for the formed citrate precursors annealed at 1000°C for 2h. The crystallite size of the formed powders was found to increase from 44.2 to 64.8 nm with increasing the Ca^{2+} ion content from 1.0 to 2.0, respectively. Meanwhile, a slightly increase in the lattice parameter "*a*" and unit cell volume were observed whereas a slightly decrease in the porosity; % was evinced as the result of increasing of Ca^{2+} ion concentration. FE-SEM observations of these powders confirmed their homogeneous regular cubic like structure. Of note, the transmittance of the sample was around 85 % with Ca^{2+} ratio 1.0. Furthermore, the band gap energy was increased from 3.8 to 4.2 eV while the DC resistivity was increased from 6.4 $x10^4$ to 6.8 $x10^4$cmΩ with calcium content. We demonstrate that without any dopant, only by controlling the chemistry and engineering, the interfacial regions at the grain boundaries, the dielectric loss was suppressed remarkably while retaining the giant dielectric constant. These investigations allow the applications of these materials in transparency, microelectronics and memory devices.

A. Introduction

Dielectric materials with high permittivity, low loss, light weight and good process ability are highly desirable for a broad range of applications including electromechanical actuators, gate dielectrics, and energy storage devices.[1-5] Although dielectric behaviour mechanism is still open to debate, a commonly accepted theory based on the internal barrier layer capacitor (IBLC) model,[6] suggested that semiconducting grains, insulating grain or domain boundaries form parallel capacitors, lead to an exceptionally high dielectric permittivity (ε'). Therefore, fine calcium copper titanate (CCTO) nanoparticles smaller than 100 nm is eagerly desired. Indeed, CCTO complex perovskite structure is very flexible, *i.e.* its dielectric constant (ε) and dielectric loss (tan δ) is highly dependent on the various cationic substitutions, such as La and Pr at Ca site or Ta, Cr, and Hf at the Ti site.[7-12] In spite of, the cationic substitution at the Cu site and its concentration in CCTO ceramic affect the dielectric properties, because Cu ion is one of the most effective inter-granular dopants for barrier layer capacitors and it can act as an acceptor ion.[13] Thereby, the presence of Cu^{1+}/Cu^{2+} ratios and their correlation with oxygen vacancies has great influence on the dielectric properties of polycrystalline CCTO via the internal barrier layer capacitance (IBLC) mechanism[14].

To date, CCTO materials are generally synthesized via two major routes, *i.e.* the conventional high-temperature solid-state reaction method[15-16] and the wet chemical methods[17-21]. In the *i.e.* solid-state reaction method, stoichiometric mixtures of $CaCO_3$, TiO_2 and CuO are usually heated up to a high temperature (1000–1150°C) for long duration (4–50h)[22]. The procedures of the solid-state synthesis are straightforward. However, the reaction products are usually not structurally and compositionally homogeneous. The solid-state reacted products often not only contain CCTO phase but also impurities such as $CaTiO_3$ and CuO were observed. Besides, it is difficult to obtain nanosized CCTO powders imputed to high annealing temperature used. The high impurity and poor powder characteristics, represented by a coarse particle size, wide particle size distribution, irregular particle morphology, and a high degree of inhomogeneity made this process unsuitable[23]. In this regard, Manik and Pradhan[24] employ the ball milling technique for synthesis of pure CCTO (18 nm) after milling for 8h. Otherwise, researchers and scientists are working for the development of high purity $CaCu_3Ti_4O_{12}$ phase with improved powder morphology, which will provide enhanced dielectric constant with low loss. Hence, wet chemistry methods are used to synthesize CCTO nanopowders including polymerized complex,[25] microwave heating,[26] sol–gel,[27] and co-precipitation methods[28].

Among these techniques, combustion route seems to be promising one as an attractive technique for the excellent chemical homogeneity, high purity and nano-sized powders. Moreover, this method has been adopted due to its many advantages compared with other methods such as energy efficiency, short reaction rate, the reagents are simple compounds, easy operable, dopants can be easily introduced into

the final product, low annealing temperature, better particle size distribution, high probability of formation of single domain and agglomeration of powders remains limited[29]. As far as we know the synthesis of CCTO powders by citrate precursor (CP) method has not been reported yet. Therefore, in this study, we investigated the details pertaining to the effect of Ca^{2+} ion variation on the crystal structure, microstructure, optical, electrical and dielectric properties of CCTO nanopowders fabricated using the citrate precursor route based on low cost effective materials. Herein, the starting materials used were citric acid, calcium carbonate, copper chloride and titanium dioxide.

B Materials and Methods

1. Materials

Anhydrous chemically grade calcium carbonate $CaCO_3$ (98.5 % Sigma Aldrich), copper chloride $CuCl_2$ (98.6%, BDH Chemical Ltd), titanium dioxide TiO_2 (99.8%, Fluka), and citric acid $C_6H_8O_7$ (98 % ADWIC) were used as starting materials. Moreover, deionized water was used in the whole work.

2. Procedure

Calcium copper titanate (CCTO) nanopowders were prepared via the citrate precursor route by mixing aqueous solutions of calcium carbonate $CaCO_3$, copper chloride $CuCl_2$ and titanium dioxide TiO_2 with Ca: Cu : Ti ratios of x:3-x:4 with different Ca^{2+} ion molar ratios (x=1.0, 1.5, and 2.0) using certain amount of citric acid. The molar ratio of metals precursor to citric acid was 1:5. The solutions were slowly heated on a hot plate with a magnetic stirring at 80°C to form viscous gel. Then, the swelled gel was dried at that temperature for 6h resulted in the dried gel citrate precursors. After that, the precursors were annealed in pure alumina crucibles at 1000 °C for 2 h in a muffle furnace (in air) with 10°C/min heating rate in order to achieve the corresponding perovskite structure in the samples.

3. Physical Characterization

X-ray powder diffraction (XRD) was carried out on a model Bruker AXS diffractometer (D8-ADVANCE Germany) with Cu Kα (λ = 1.54056 Å) radiation, operating at 40 kV and 40 mA. The diffraction data were recorded for 2θ values between 10° and 80°. Scanning electron microscopy was performed by a FE-SEM (JEOL-JSM-5410 Japan). The UV-Vis absorption spectrum was measured by UV-VIS-NIR-scanning spectrophotometer (JASCO V-570 spectrophotometer, Japan). An electrometer and DC power supply (Agilent-4339B, USA) were used for the electrical resistivity measurement. Dielectric properties were measured using a network impedance analyzer (Agilent-E4991A, USA) in the frequency range of 1 MHz to 3 GHz.

C. Results and Discussion

1. Synthesis of CCTO nanopowders

XRD patterns of $Ca_xCu_{3-x}Ti_4O_{12}$ (x = 1.0, 1.5 and 2.0) powders synthesized by the citrate precursors process calcined at 1000°C for 2h are shown in Figure 1. The main peaks of calcined $Ca_xCu_{3-x}Ti_4O_{12}$ powders are assigned to pure $Ca_xCu_{3-x}Ti_4O_{12}$ (JCPDS card no.75-2188). Peaks belonging to (200), (211), (220), (013), (222), (321), (400), (422), (440), (433), and (620) planes of cubic CCTO phase were indexed. No extra secondary impurity phases were detected with increasing Ca^{2+} ions content[30-32]. Weak diffraction peaks observed on Figure 1 are not corresponding to secondary phases but it is noise due to the granular morphologies of CCTO sample. It is clear that the samples with large Ca^{+2} ion concentrations exhibited a small shift in the XRD peaks towards larger 2θ (Figure SI1). The shift was increased with increasing Ca^{+2} ion content corresponding to a decrease of the distances between the crystalline planes.

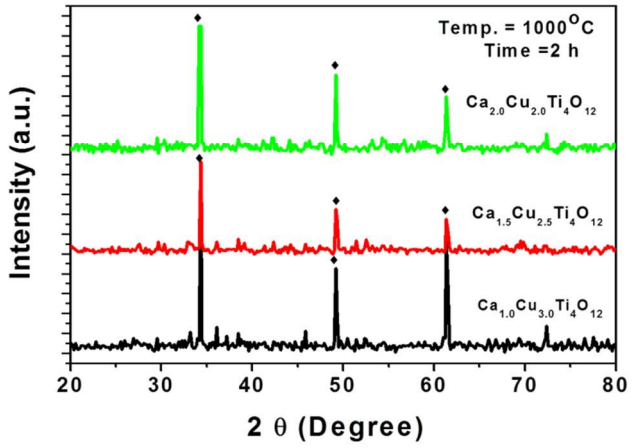

Fig. 1 XRD patterns of CCTO nanopowders with different Ca^{2+} ion content 1.0, 1.5, and 2.0 prepared by citrate precursor method and annealed at 1000°C for 2h

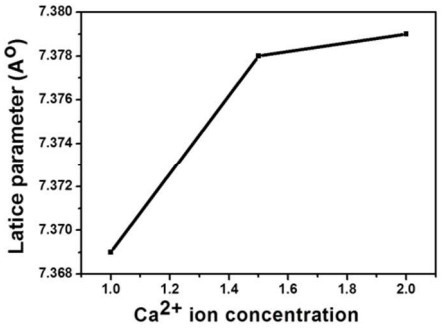

Fig. 2 Lattice constant of CCTO nanopowders as a function of Ca^{2+}concentrations

The lattice parameter (a) and the unit cell volume (V_{cell}) for the cubic perovskite structure were calculated using the following equations:[18]

$$dhkl = \frac{a}{\sqrt{h^2+k^2+l^2}} \qquad (Equation\ 1)$$

$$Vcell = a^3 \qquad (Equation\ 2)$$

The X-ray density (dx) was calculated using the following equation:

$$dx = \frac{NM}{(NA\ Vcell)} \qquad (Equation\ 3)$$

Where N is the number of molecules per unit cell, N = 1 for CCTO, and the Avogadro's number NA = 6×10^{23}.

The apparent density (d_m) was measured in bidistilled water according to Archimedes's principle using the following relation:

$$dm = \left[1 - \left(\frac{ms}{mw}\right) * dw\right] \quad (Equation\ 4)$$

Where m_s the mass of the sample in air, m_w is the mass of the sample in water and d_w is the density of water (1g/cm^3). The material porosity (P) was calculated using the following relation:

$$P = \left[1 - \left(\frac{dm}{dx}\right)\right] * 100 \quad (Equation\ 5)$$

Table 1. Structural parameters of the produced ($Ca_xCu_{3-x}Ti_4O_{12}$) powders with different Ca^{2+} ioncontent

Ca^{2+}ion content	Crystallite size (nm)	Lattice parameter(Å) ***a***	Unit cell volume(Å^3)	App. Density d_m (g/cm^3)	X-ray density d_x (g/cm^3)	Porosity, P (%)
1.0	**44**	7.369± 0.001	400.152	3.859	5.052	23.61
1.5	**52**	7.378± 0.001	401.620	3.950	5.154	23.36
2.0	**64**	7.379± 0.001	401.783	3.997	5.215	23.31

The variation in the structural parameters such as crystallite size, lattice constant "*a*", X-ray density (d*x*) and the porosity is given in Table 1. Lattice parameter was slightly increased with increasing Ca^{2+} ion content. This is due to larger ionic radii of Ca^{2+} ion (1.14 Å) as compared to Cu^{2+} ion (0.87 Å). Hence, the unit cell volume was increased from 400.15 to 401.78 Å^3 by increasing calcium ion concentration from 1.0 to 2.0. Furthermore, the apparent density for all prepared samples was smaller than that calculated with X-ray density. Beside, the percentage of porosity was decreased with increasing *x* value of Ca^{2+} ion.

Figure 3 shows the SEM images of the CCTO powders prepared by citrate precursor method calcined at 1000^{o}C for 2h. All microphotographs show nanosize particles, which gradually change their shape with the increase of Ca^{2+} ion molar ratios. All particles displayed cubic like structure with grain size ranging between 50 and 100 nm. Observing from Figure 3b and 3c micrographs, we can verify the formation of necks between the initial touching particles with formation of elongated particles, which cause the growth of $Ca_xCu_{3-x}Ti_3O_{12}$ particles relatively to the amount of Ca^{2+} ion content. Moreover, all samples have a homogeneous microstructure consisting of equiaxed grains. There was no significant difference in the microstructures of the CCTO. It can be seen the irregularly shaped crystallites are formed with different sizes, as shown in Figure 3a. For the ***x***=1.5 and 2.0 samples, the grains have largely grown as shown in Figure 3b and 3c. The largest and some smaller grain size are even larger than that of CCTO sample with 0.5 Ca^{2+} content. Energy dispersive X-ray (EDX) analysis of $Ca_xCu_{3-x}Ti_4O_{12}$ (x=1.0) nanopowders calcined at 1000^{o}C in air for 2 h prove the absence of any impurity peaks in the EDS spectrum. The close similitude of the atomic ratios of Ca, Cu and Ti to the nominal composition in $Ca_xCu_{3-x}Ti_4O_{12}$ proves the elemental and phase purity of the prepared samples.[23, 28]

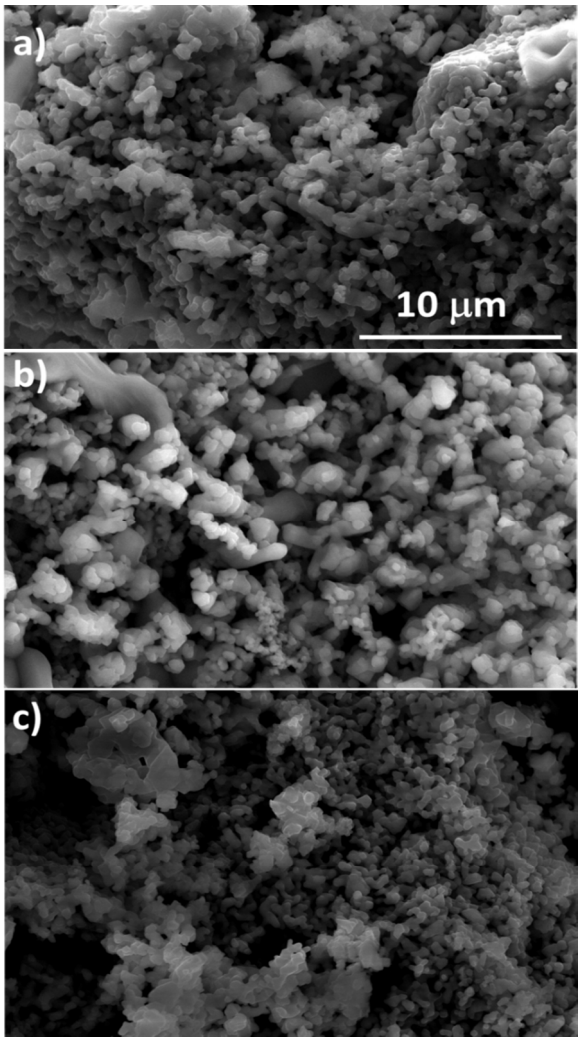

Fig. 3: Scanning electron microphotographs for $Ca_xCu_{3-x}Ti_4O_{12}$ at different Ca^{2+} ion content (a) 1.0 (b) 1.5 and (c) 2.0

Optical properties

The optical properties of the synthesized CCTO particles annealed at 1000°C for different Ca^{+2} molar ratios were examined by UV-Vis spectrophotometer and the results are depicted in Figure 4. For the measurement, the synthesized powders were well dispersed in distilled water and the resultant solutions were used for the measurement. The transmittance T% spectrum recorded for the as prepared CCTO particles in the range of 200–800 nm (Reflectance in SI2) is given in Figure 4b. All samples showed transmittance increased over 35 % by the increasing of Ca^{2+} ions content in the wavelength range between 200 nm and 800 nm.

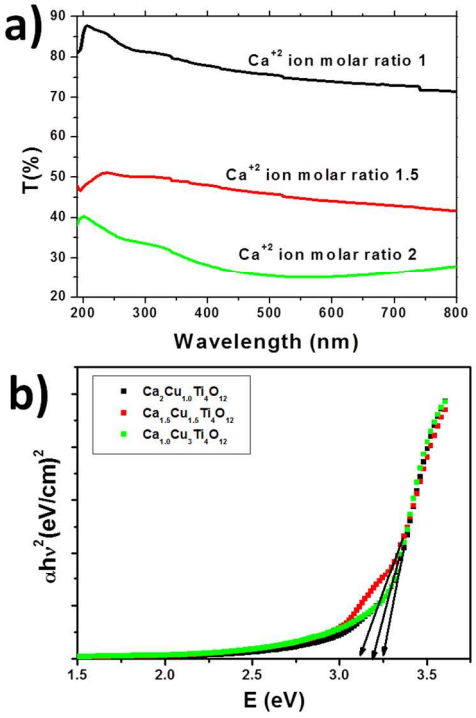

Fig. 4 a) UV–visible transmittance spectrum (T%) of ($Ca_{1-x}Cu_xTi_4O_{12}$) nanopowders synthesized using citrate precursor method annealed at 1000°C for 2h using different Ca^{2+} ion content (1.0, 1.5and 2.0); b) The band gap energy of CCTO at different Ca^{+2} ion content (1.0, 1.5, and 2.0).

The well structured and smooth oscillations of the transmittance profiles indicate that all samples have flat surfaces and uniform size. The band gap energy was determined by extrapolating of the absorption coefficient (α) to zero from the spectral data. The absorption coefficient was calculated by the following equation

$$(\alpha h\upsilon)^m = h\upsilon - E_g \qquad (Equation\ 6)$$

Where α is the absorption coefficient, hυ is the photon energy, E_g is the band gap energy, m=1/2 or 3/2 for indirect allowed and indirect forbidden transitions, and m=2 or 3 for direct allowed and direct forbidden transitions.

Liu *et al.*[18] describes that the band gap energy is direct when the electronic transitions occur from the maximum-energy states (near or inside) the valence band (VB) to minimum-energy states (below or inside) the conduction band (CB), in the same regions in the Brillouin zone. Therefore, the presence of different E values calculated from the UV-Vis absorption spectra indicates the existence of intermediary energy levels between the valence and the conduction band[29]. The band gap energy was estimated by plotting $(\alpha h\upsilon)^2$ of the CCTO against the photon energy (hυ). The linear relationship between $(\alpha h\upsilon)^2$ and hυ supports the model of direct allowed band electronic transition. The band gap energy was determined by extrapolating the absorption coefficient (α) to zero. The absorbance (A) is converted to the absorption coefficient using the following relationship[24].

$$\alpha = \frac{(2.303\times10^3)A\rho}{lc} \qquad (Equation\ 7)$$

Where A is the absorbance of the sample, ρ is the density of CCTO, l is the length (1 cm), and c is the concentration of the CCTO nanocrystals. By plotting $(\alpha h\nu)^2$ vs. hν, the optical band-gaps (Eg) of the samples were realized as the intercepts with x-axis, as shown in Figure 4. For $Ca_xCu_{3-x}Ti_4O_{12}$ (x = 1.0, 1.5 and 2.0), the band-gap energies were found to be 3.12, 3.20, and 3.26 eV, respectively. The Eg increased with increasing Ca^{2+} ion content. The electronic transitions occur inside the $Ca_xCu_{3-x}Ti_4O_{12}$ microcrystals (Figure 4). The 3d orbitals of the copper atoms will be associated to the conduction band,[27] so a decrease of the optical gap is observed. Moreover, structural defects such as distortions and/or strains in the $CaTiO_3$ lattice caused by the introduction of copper in these systems are able to induce the symmetry break of the [TiO_6] and [CaO] leading to an appearance of intermediary levels between the valence and conductions bands [25, 26,30].

Electrical resistivity

The effect of calcium ion on the DC resistivity of CCTO was investigated. Table 2 presents the variation of DC resistivity versus Ca^{2+} ion content. It is observed that the DC resistivity was markedly dependent on the Ca ions substitutions. The room temperatures resistivity was increased with the increasing of the Ca^{2+} content, most of probably due to the high degree of crystallization observed in the XRD and the low mobility of the Ca^{2+} ions.

Table 2. Variation of DC resistivity versus Ca^{2+} ion content

Ca^{2+} ion content	1.0	1.5	2.0
ρ (Ωcm)	6.4×10^4	6.6×10^4	6.8×10^4

Dielectric studies

Fig. 5 shows the plots of variations in dielectric constant of the real part (ε'), imaginary part (ε″), and dielectric loss (tanδ) measured for the silver painted samples, at room temperature, over the frequency range 1MHz to 3 GHz. The high dielectric constant values obtained at the high frequency region, are as high as those reported by other authors like Masingboon *et al.*[19], Jin *et al.*[17] and Liu *et al.*[23]. They also prepared CCTO samples using wet chemical methods. At room temperature it is seen that, for all the samples, drops approximately for frequencies higher than 1 GHz. The analysis of complex permittivity dependence with frequency, at room temperature, shows the existence of two

relaxation processes for all the samples. The high and low frequency relaxations are usually associated with the grain and grain boundary dielectric response,[32-33] respectively.

The porosity of materials directly affects the dielectric characteristics such as real and imaginary permittivity. It is possible that dielectric constant increases with larger grain size. Densification of sample also plays a major part in contributing to the value of dielectric constant of CCTO. Porous sample will make dielectric more difficult to penetrate and also dissipate more heat which will reduce the dielectric constant of the sample.[34-35]

The frequency dependent dielectric constant (ε'), (ε'') and dielectric loss (tanδ) at room temperature for the samples, Ca^{2+} 1.0, Ca^{2+} 1.5 and Ca^{2+} 2.0 are shown in Figure 5. The dielectric constant value obtained for Ca^{2+} 1.0 samples is around $0.02x10^3$ at 1.5 GHz and increased to $0.05x10^3$ as the frequency increased to 1.75 GHz then decreased with the frequency increased.

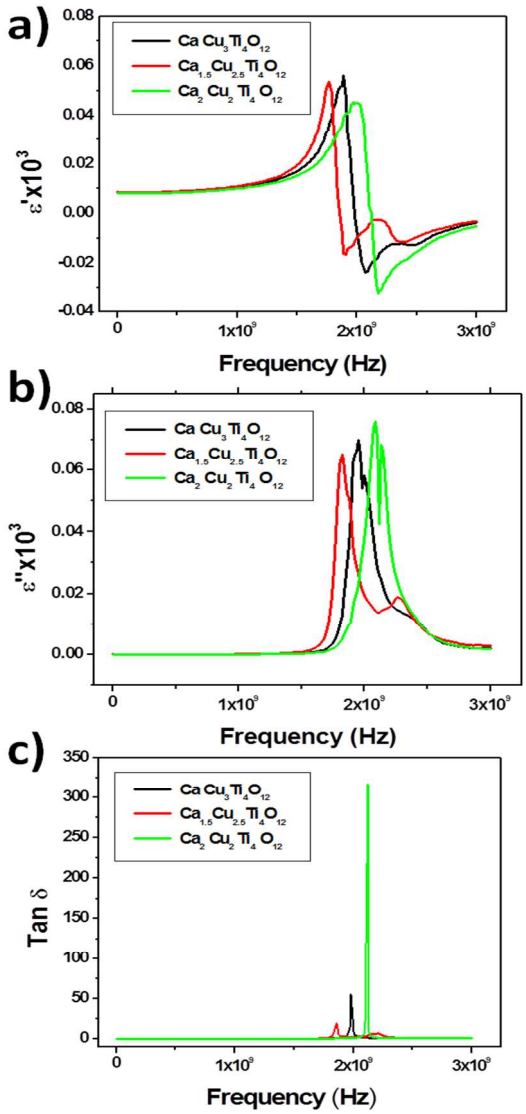

Fig. 5: (a) Frequency-dependent of the real part permittivity , (b) imaginary part permittivity and (c) loss factor (tanδ) of $CaCu_3Ti_4O_{12}$nanopowders with silver-paint contacts prepared by citrate precursor with different Ca^{+2} ion content.

The Ca^{2+} 1.5 sample, which has higher calcium content (by 0.5 mol %) exhibited a dielectric constant value of around $0.05x10^3$ at 1.65 GHz. The Ca^{2+} 1.5 sample shows low frequency dispersion as compared to that of Ca^{2+} 1.0 samples. Interestingly, the Ca^{2+} 2.0 sample, which is higher calcium content exhibited very low dielectric constant as compared to that of other samples (Ca^{2+} 1.0 and Ca^{2+} 1.5) at all the frequencies under study. The loss factor varies with the change of calcium ion content. The higher calcium ions content has the higher loss factor compared to the other samples. The dielectric loss did not show any relaxation at low frequency, though there is a relaxation at high frequency.

The dielectric loss values obtained for Ca 1.0 (at 1.8 GHz) is 25 and for Ca 1.5 (at 2.0 GHz) is 50. For the rich calcium sample it will be 300 at 2.3 GHz. It is to be noted that the calcium deficient sample (Ca^{2+} 1.0), exhibited low dielectric loss, while retaining the high dielectric constant. It is known in the literature that various dopants were used to bring down the dielectric loss in CCTO[18-19, 23-25, 27, 29].The dielectric losses reported in this study are slightly high. This may be attributed to the porosity of the materials and the measurement of the dielectric losses in high frequency range (Gigahertz range). However this is matches the frequency range measurements and the value reported by Fritsch *et al.*[16]

The reduction in the dielectric loss in CCTO also affected the dielectric constant to a large extent. However, in this work, without any dopant, only by controlling the chemistry and engineering the interfacial regions at the grain boundaries, the dielectric loss was suppressed remarkably while retaining the giant dielectric constant.

Works are in progress in order to measure dielectric breakdown field strength as the function of different Ca^{2+} content.

Conclusions

In this study, pure $Ca_xCu_{3-x}Ti_4O_{12}$ nanopowders were successfully synthesized through citrate precursor route using low cost starting materials. The crystallite size varies from 44.2 to 64.8 nm as the result of increasing Ca^{2+} ion content. The microstructure of the formed powders appeared as cubic like structure. The high transparency of the formed $Ca_xCu_{3-x}Ti_4O_{12}$ was considered with Ca^{2+} ions content of 1.0. Of note, the band gap energy was increased with increasing Ca^{2+} ion concentrations. For instance, it was increased from 3.12 to 3.26 eV by increasing the Ca^{2+} ion ratio from 1.0 to 2.0. Meanwhile, the imaginary part of complex permittivity and dielectric loss factor were increased with increasing Ca^{2+} ion content. These results indicate that the CCTO is a future material in electronic applications such as capacitors, memory device, resonators and filters.

Notes and references

[a]*Central Metallurgical Research and Development Institute, P.O. Box: 87 Helwan, Cairo, Egypt*

[b]*Chemistry Department, Faculty of Science, Taif University, P.O. Box: 888, Al-Haweiah, Taif-Saudi Arabia*

[c]*Institut Européen des Membranes, UMR 5635 ENSCM UM2 CNRS, Université Montpellier 2, Place Eugène Bataillon, 34095 Montpellier, France*
Corresponding author: ali_omar155@yahoo.com

This work was partially supported by the French Government through a fellowship granted by the French Embassy in Egypt (Institute francais d'Egypt).

1. F. Carpi, G. Gallone, F. Galantini and D. De Rossi, *Advanced Functional Materials*, 2008, **18**, 235-241.
2. C. Huang and Q. M. Zhang, *Advanced Materials*, 2005, **17**, 1153-1158.
3. P. Kim, X.-H. Zhang, B. Domercq, S. C. Jones, P. J. Hotchkiss, S. R. Marder, B. Kippelen and J. W. Perry, *Applied Physics Letters*, 2008, **93**, -.
4. K. H. Lee, J. Kao, S. S. Parizi, G. Caruntu and T. Xu, *Nanoscale*, 2014, **6**, 3526-3531.
5. Q. M. Zhang, H. Li, M. Poh, F. Xia, Z. Y. Cheng, H. Xu and C. Huang, *Nature*, 2002, **419**, 284-287.
6. W. L. Li, Y. Zhao, Q. G. Chi, Z. G. Zhang and W. D. Fei, *RSC Advances*, 2012, **2**, 6073-6078.
7. B. Cheng, Y.-H. Lin, J. Yuan, J. Cai, C.-W. Nan, X. Xiao and J. He, *Journal of Applied Physics*, 2009, **106**, -.
8. M. A. de la Rubia, P. Leret, A. del Campo, R. E. Alonso, A. R. López-Garcia, J. F. Fernández and J. de Frutos, *Journal of the European Ceramic Society*, 2012, **32**, 1691-1699.
9. L. Feng, X. Tang, Y. Yan, X. Chen, Z. Jiao and G. Cao, *physica status solidi (a)*, 2006, **203**, R22-R24.
10. Q. Zheng, H. Fan and C. Long, *Journal of Alloys and Compounds*, 2012, **511**, 90-94.
11. P. Kum-onsa, P. Thongbai, B. Putasaeng, T. Yamwong and S. Maensiri, *Journal of the European Ceramic Society*, 2015, **35**, 1441-1447.
12. L. Singh, U. S. Rai, K. D. Mandal and A. Rai, *Appl. Phys. A*, 2013, **112**, 891-900.
13. L. Singh, I. W. Kim, B. C. Sin, K. D. Mandal, U. S. Rai, A. Ullah, H. Chung and Y. Lee, *RSC Advances*, 2014, **4**, 52770-52784.
14. L. Cao, P. Liu, J.-P. Zhou, Y.-J. Wang, L.-N. Su, C. Liu and H.-W. Zhang, *Journal of Ceramic Processing Research*, 2010, **11**, 453-459.
15. W. X. Yuan, S. K. Hark and W. N. Mei, *Journal of Ceramic Processing Research*, 2009, **10**, 696-699.
16. S. Guillemet-Fritsch, T. Lebey, M. Boulos and B. Durand, *Journal of the European Ceramic Society*, 2006, **26**, 1245-1257.
17. S. Jin, H. Xia, Y. Zhang, J. Guo and J. Xu, *Materials Letters*, 2007, **61**, 1404-1407.
18. J. Liu, R. W. Smith and W.-N. Mei, *Chemistry of Materials*, 2007, **19**, 6020-6024.
19. C. Masingboon, P. Thongbai, S. Maensiri, T. Yamwong and S. Seraphin, *Materials Chemistry and Physics*, 2008, **109**, 262-270.
20. C. Puchmark and G. Rujijanagul, *Ferroelectrics*, 2011, **415**, 107-112.
21. C.-M. Wang, K.-S. Kao, S.-Y. Lin, Y.-C. Chen and S.-C. Weng, *Journal of Physics and Chemistry of Solids*, 2008, **69**, 608-610.
22. S. K. Manik and S. K. Pradhan, *Physica E: Low-dimensional Systems and Nanostructures*, 2006, **33**, 160-168.
23. L. Liu, H. Fan, P. Fang and X. Chen, *Materials Research Bulletin*, 2008, **43**, 1800-1807.
24. A. K. Rai, N. K. Singh, S.-K. Lee, K. D. Mandal, D. Kumar and O. Parkash, *Journal of Alloys and Compounds*, 2011, **509**, 8901-8906.
25. S. Jesurani, S. Kanagesan, T. Kalaivani and K. Ashok, *J Mater Sci: Mater Electron*, 2012, **23**, 692-696.
26. J. Liu, Y. Sui, C.-g. Duan, W.-N. Mei, R. W. Smith and J. R. Hardy, *Chemistry of Materials*, 2006, **18**, 3878-3882.
27. M. M. Rashad, A. O. Turky and A. T. Kandil, *J Mater Sci: Mater Electron*, 2013, **24**, 3284-3291.
28. D. Xu, K. He, R. Yu, X. Sun, Y. Yang, H. Xu, H. Yuan and J. Ma, *Materials Chemistry and Physics*.
29. B. Barbier, C. Combettes, S. Guillemet-Fritsch, T. Chartier, F. Rossignol, A. Rumeau, T. Lebey and E. Dutarde, *Journal of the European Ceramic Society*, 2009, **29**, 731-735.
30. P. Mishra and P. Kumar, *Ceramics International*, 2015, **41**, 2727-2734.
31. M. A. Ponce, M. A. Ramirez, F. Schipani, E. Joanni, J. P. Tomba and M. S. Castro, *Journal of the European Ceramic Society*, 2015, **35**, 153-161.
32. S. I. R. Costa, M. Li, J. R. Frade and D. C. Sinclair, *RSC Advances*, 2013, **3**, 7030-7036.
33. R. Schmidt, S. Pandey, P. Fiorenza and D. C. Sinclair, *RSC Advances*, 2013, **3**, 14580-14589.
34. L. Singh, I. W. Kim, B. Cheol Sin, A. Ullah, S. Kook Woo and Y. Lee, *Materials Science in Semiconductor Processing*, 2015, **31**, 386-396.
35. A. K. Rai, J. Gim, E.-c. Shin, H.-H. Seo, V. Mathew, K. D. Mandal, O. Parkash, J.-S. Lee and J. Kim, *Ceramics International*, 2014, **40**, 181-189.

Graphical abstract

The present study acts as a simple and effective way in synthesis and characterization of CCTO with tunable optical and dielectrical properties